UCRL-CONF-227881

LAWRENCE
LIVERMORE
NATIONAL
LABORATORY

SYNTHESIS AND PERFORMANCE OF FE-BASED AMORPHOUS ALLOYS FOR NUCLEAR WASTE REPOSITORY APPLICATIONS

L. Kaufman, J.H. Perepezko, K. Hildal

February 8, 2007

Disclaimer

SYNTHESIS AND PERFORMANCE OF FE-BASED AMORPHOUS ALLOYS FOR NUCLEAR WASTE REPOSITORY APPLICATIONS

L. Kaufman
Larry Kaufman
140 Clark Road
Brookline, MA, 02445-5848
larrykaufman@rcn.com

J.H. Perepezko and K Hildal
Department of Materials Science and Engineering
University of Wisconsin-Madison
1509 University Ave.
Madison, WI 53706
perepezk@engr.wisc.edu, hildal@wisc.edu

ABSTRACT

In several Fe-based alloy systems it is possible to produce glasses with cooling rates as low as 100 K/s that exhibit outstanding corrosion resistance compared to typical crystalline alloys such as high-performance stainless steels and Ni-based C-22 alloy. Moreover, novel alloy compositions can be synthesized to maximize corrosion resistance (i.e. adding Cr and Mo) and to improve radiation compatibility (adding B) and still maintain glass forming ability. The applicability of Fe-based amorphous coatings in typical environments where corrosion resistance and thermal stability are critical issues has been examined in terms of amorphous phase stability and glass-forming ability through a coordinated computational analysis and experimental validation. Similarly, a novel computational thermodynamics approach has been developed to explore the compositional sensitivity of glass-forming ability and thermal stability. Also, the synthesis and characterization of alloys with increased cross-section for thermal neutron capture will be outlined to demonstrate that through careful design of alloy composition it is possible to tailor the material properties of the thermally spray-formed amorphous coating to accommodate the challenges anticipated in typical nuclear waste storage applications over tens of thousands of years in a variety of corrosive environments.

Key Words: Computational Thermodynamics, Alloy Design, Amorphous Alloys, Corrosion Resistance, nuclear waste repository

1. INTRODUCTION

Recent developments in multicomponent Fe-based amorphous alloys have shown that these novel materials exhibit outstanding corrosion resistance compared to typical crystalline alloys such as high-performance stainless steels and Ni-based C-22 alloy. During the past decade, amorphous alloy synthesis has advanced to allow for the casting of bulk metallic glasses. In several Fe-based alloy systems it is possible to produce glasses with cooling rates as low as 100 K/s. At such low cooling rates, there is an opportunity to produce amorphous solids through industrial processes such as thermal spray-formed coatings. Moreover, since cooling rates in typical thermal spray processing exceed 1000 K/s, novel alloy compositions can be synthesized

to maximize corrosion resistance (i.e. adding Cr and Mo) and to improve radiation compatibility (adding B) and still maintain good glass-forming ability.

In this work the applicability of Fe-based amorphous coatings in typical environments where corrosion resistance and thermal stability are critical issues has been examined in terms of amorphous phase stability and glass-forming ability through a coordinated computational analysis and experimental validation. For example, a wedge casting technique has been applied to examine bulk glass forming alloys by combining multiple thermal probes with a measurement based kinetics analysis and a computational thermodynamics evaluation to elucidate the phase selection competition and critical cooling rate conditions [1].

2. COMPUTATIONAL APPROACH

Two basic strategies are being examined for the evaluation of the thermal stability of the amorphous phase with regard to crystallization. In one approach, the measured onset time for the nucleation of crystallization during isothermal annealing of initially amorphous samples is used as input to evaluate some of the parameters in a nucleation model that is then applied to compute a time-temperature transformation (TTT) diagram over the entire temperature range between T_g, the glass transition temperature and the onset of melting, T_m. The resultant TTT diagram is converted into a continuous cooling transformation diagram that is further constrained by the requirement that it must be consistent with the measured critical cooling rate range for glass formation. For the second approach, a computational kinetics program, DICTRA, together with a computational thermodynamics program, THERMOCALC, is applied to evaluate the crystallization kinetics. In this method, experimental data on the size and number density of crystallites following thermal treatment is used as input as well as an assessment of the atomic mobility database for the amorphous alloy composition under consideration. The computational kinetics program then yields the time for dissolution of the crystallites at each temperature to evaluate the nucleation time that is necessary for the TTT diagram. In both approaches the thermodynamic database and THERMOCALC are employed to assess the relevant driving free energies that are necessary for the nucleation and growth kinetics computations.

3. GLASS FORMATION AND THERMAL STABILITY

Based upon direct measurements and kinetics modeling it is evident that a critical cooling rate range should be considered to account for nucleation behavior and that the relative heat flow characteristics as well as nucleation kinetics are important in judging ease of glass formation. As indicated in micrograph in Fig.1 that reveals the cross section of a wedge-casting sample for a (SAM 35) alloy [see Table 1 for alloy compositions], the transition from an amorphous phase (top) to a crystalline phase mixture (bottom) does not occur at a single cooling rate. Instead, due to the stochastic nature of nucleation there is a range of cooling rates for the glass to crystal transition.
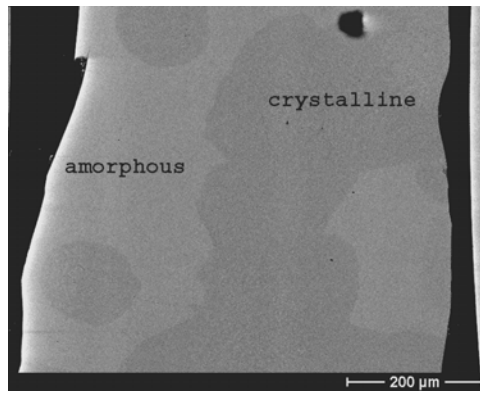
Joint International Topical Meeting on Mathematics & Computation and
Supercomputing in Nuclear Applications (M&C + SNA 2007), Monterey, CA, 2007

2/13

Figure 1. Back-Scattered Electron image of wedge-cast SAM 35 alloy.

From thermal measurements during wedge-casting and the application of a finite difference heat flow analysis the cooling rate range for glass formation can be determined accurately [1,2]. Supplementary isothermal nucleation kinetics measurements by differential scanning calorimetry (DSC) and crystallization phase identification by X-ray diffraction and transmission electron microscopy provide key input data for a competitive nucleation model. The full evaluation of the nucleation kinetics model requires the thermodynamic driving free energy that is obtained from Thermocalc which is a comprehensive computational thermodynamics tool. The Thermocalc analysis also provides useful guidance in the interpretation of devitrification reactions in the form of a phase fraction plot as a function of temperature (Fig.2).
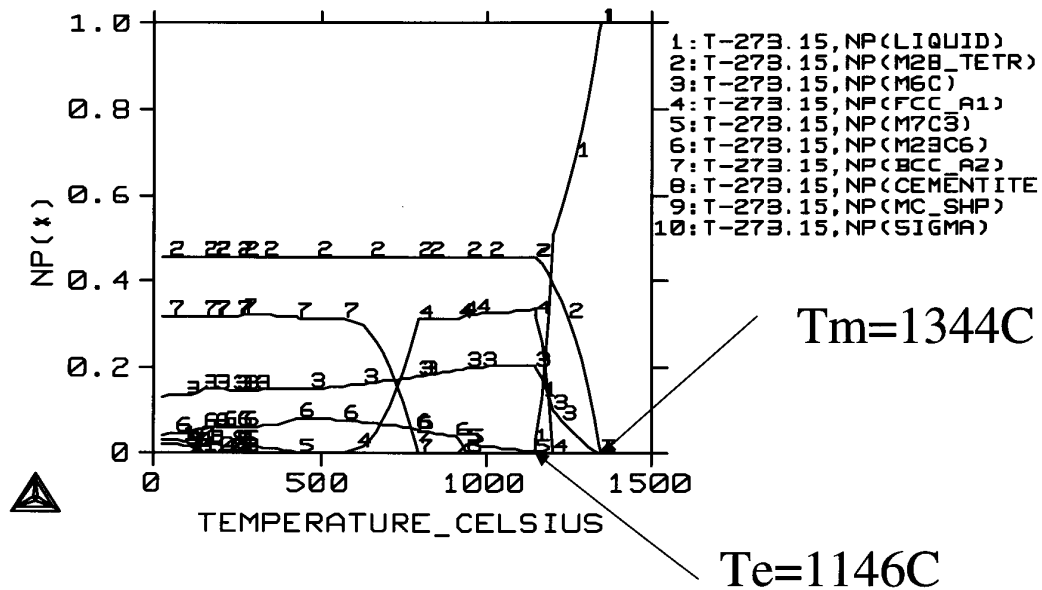

Figure 2. Phase fraction, NP vs. temperature calculated for SAM 2X5.

Based on classical nucleation theory for heterogeneous nucleation the steady-state nucleation rate J can be expressed as [3]

$$J = \Omega \exp\left[\frac{-\Delta G^* f(\theta)}{kT}\right] \tag{3}$$

where k is Boltzmann`s constant, $f(\theta)$ is a catalysis factor, with a range $0 \leq f(\theta) \leq 1$. For spherical nuclei $f(\theta) = (2 - 3\cos\theta + \cos^3\theta)/4$, where θ is the contact angle between the nucleus and the catalytic substrate. The prefactor term can be expressed as [4]

$$\Omega = \rho_s \nu = \rho_s D_L / d^2 \tag{4}$$

where ρ_s = available site density, ν = attachment frequency, D_L = liquid diffusivity and d = jump distance, i.e. 0.3 nm. The activation barrier for nucleation of a spherical nucleus, ΔG^*, is obtained from classical theory as

$$\Delta G^* = (16\pi/3)\left(\sigma^3 / \Delta G_v^2\right) \tag{5}$$

where $16\pi/3$ is a geometrical factor characteristic for the formation of a spherical nucleus, σ is the interfacial energy between liquid and solid and ΔG_v is the free energy difference between the liquid and crystalline phases. The approach to the determination of the appropriate value for ΔG_v is dependent on the mode of the crystallization reaction that is competing with glass formation during cooling. For a polymorphous or eutectic mode of crystallization where the product phases have the same overall composition as the liquid, the value of ΔG_v is determined by the vertical separation between the liquid curve and the solid curve in figure 2 (i.e. separation a-b for polymorphous or a-c for eutectic). When primary phase formation controls the initial crystallization reaction, the primary phase nucleus composition that is favored can be assessed by a parallel tangent construction that is identified by the distance a-d in figure 2.

The onset of crystallization is defined as when a nucleation event occurs within a volume V at a given temperature T after a crystallization time t by

$$JVt = 1 \tag{6}$$

The diffusion coefficient that is used to evaluate the attachment frequency for nucleation is often obtained by the relation between the diffusivity to the viscosity through the Stokes-Einstein equation [5], by assuming that diffusion and viscous flow occur with the same mechanism that is based on Brownian motion:

$$D_L = \frac{kT}{3\pi a \eta} \tag{7}$$

where η is the kinematic viscosity and a is taken as an atomic size. This correlation is widely used to introduce viscosity into the nucleation rate equation, however, it should be noted that there is evidence, mostly collected with molecular glass-formers, that equation (7) does not hold for temperatures around T_g, but starts to fail around 1.2-1.3 T_g [6]. A Vogel-Fulcher-Tamann relation [7] was used to express the viscosity as a function of temperature:

$$\eta = A\exp\left[\frac{B}{T-T_0}\right] \tag{8}$$

where A and B are constants, and T_0 is the temperature at which the excess configurational entropy is zero (Kauzmann temperature). T_0 is somewhat lower than T_g measured during continuous heating, and the parameter B is typically of the order 10^3 for a broad range of metallic glasses [8], however, for the alloy systems considered in this work no experimental data on viscosity exists.

Inserting equations (3)-(5) and (7)-(8) into (6), the following expression linking the onset time for nucleation to the temperature is acquired as:
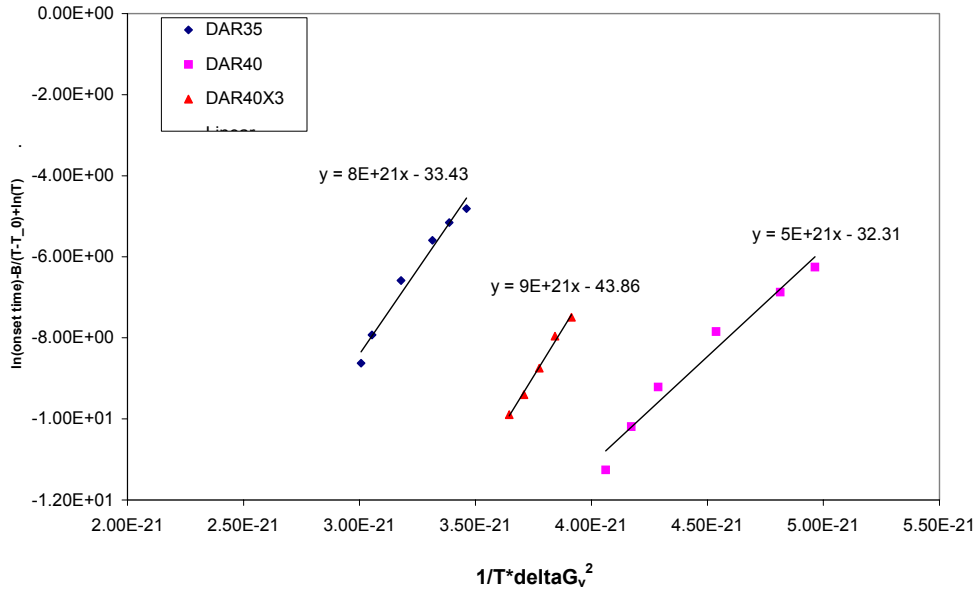
$$\ln(t) = \Gamma + \frac{B}{T-T_0} - \ln T + \frac{C}{T\Delta G_v^2} \tag{9}$$

The prefactor $\Gamma = \ln(3\pi a^3 A/\rho_s Vk)$ is assumed independent of temperature. The constant C represents part of the nucleation barrier and is given by $C=(16\pi/3k)\sigma^3 f(\theta)$. Rearranging equation (9) yields

$$\ln(t) - \frac{B}{T-T_0} + \ln T = \Gamma + \frac{C}{T\Delta G_v^2} \tag{10}$$

The onset times for crystallization are defined by the intersection of the baseline tangent and the inflection point tangent of the crystallization peak during isothermal annealing of as-spun ribbons using DSC. The onset times are used in equation (10) to evaluate Γ and C by plotting the left hand side of equation (10) as a function of $1/T\Delta G_v^2$. This is illustrated in figure 3. The TTT-curve can now be constructed for a given set of viscosity parameters B and T_0, assuming that C is independent of temperature.

Although the fit to the data resulting from the isothermal annealing seems quite good, it must be emphasized that the temperature range over which the data were acquired is relatively narrow (30-35 K) and as such any temperature dependence of the interfacial energy that is part of the expression for C is not easily captured with this approach. The result of this analysis is a Time-Temperature-Transformation (TTT) diagram such as that shown in figure 4 for a (SAM 40) alloy.

Joint International Topical Meeting on Mathematics & Computation and
Supercomputing in Nuclear Applications (M&C + SNA 2007), Monterey, CA, 2007

5/13

Figure 3. A plot of equation (10) which yields the value for *C* (the slope of the linear fit to the data) for three Fe-based amorphous alloys.
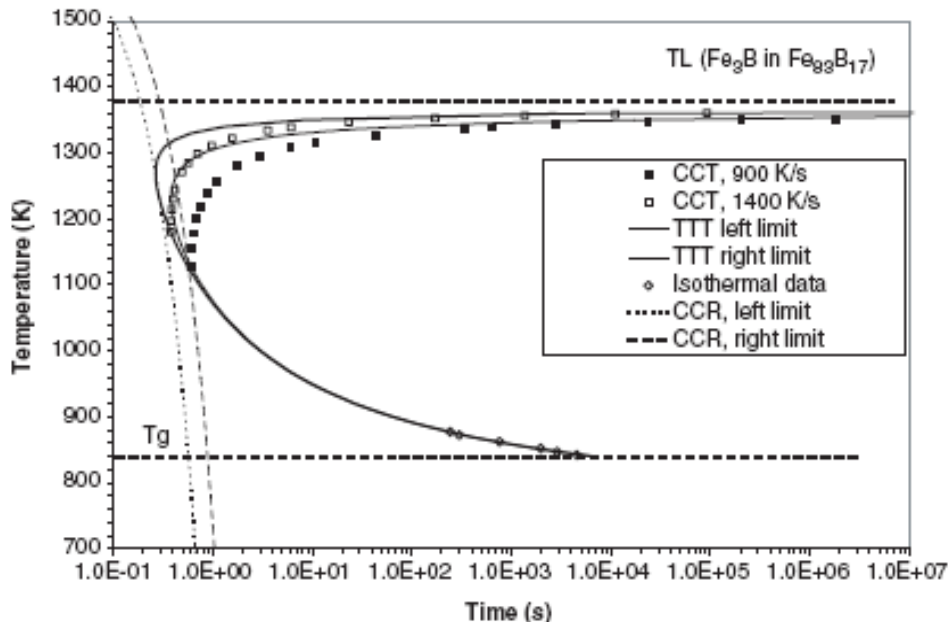

Figure 4. Isothermal onset times for crystallization, critical cooling rate range and the calculated TTT curve for the initial crystallization of the Fe₃B structure type phase in SAM 40 alloy.

Joint International Topical Meeting on Mathematics & Computation and Supercomputing in Nuclear Applications (M&C + SNA 2007), Monterey, CA, 2007

6/13

While the initial analysis result is valuable, it is based upon a limited dataset for evaluation. He kinetic model does allow for extrapolation to the long times that are necessary to determine the amorphous phase stability for nuclear repository conditions. However, the uncertainty in some of the parameters that were estimated for the initial analysis will require further work to obtain reliable long-term stability predictions.

In a complementary effort a computational approach is being pursued that is based upon DICTRA. The DICTRA method is a kinetic model analysis that incorporates the Thermocalc database together with an atomic mobility database. With the DICTRA method the full diffusion matrix including the cross term members in a multicomponent alloy can be obtained as input to a crystal growth kinetics analysis. With minimal experimental data such as the product phase identity and the product phase size and number density DICTRA provides an analysis of the crystallization onset as a TTT diagram that is shown in Fig. 5 for the SAM 7 alloy. The DICTRA method and the nucleation kinetics analysis model are being used in a complementary way to provide an integrated analysis for a robust thermal stability assessment.
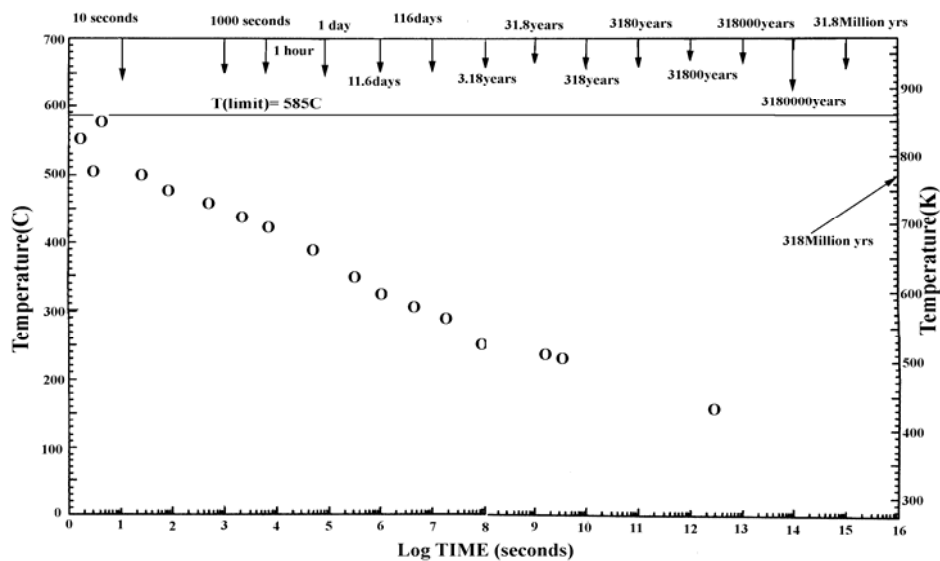

**Figure 5. Calculated TTT curve for the onset of crystallization of SAM 7 to an M$_3$B phase based upon DICTRA.**

4. ANALYSIS OF CORROSION PERFORMANCE

The Thermocalc database and computational tools have been adapted to provide guidance in the design of engineering alloys for enhanced corrosion resistance. For example, Fig.6 presents the computational results for the relative abundance (i.e. phase fraction) vs. corrosion potential for a given PH=6.4 that is typical of 90°C seawater. The abundance and corrosion potential range of passive surface layers such as Cr$_2$O$_3$ can be optimized for given corrosion conditions by controlling the multicomponent alloy composition.

Similarly the corrosion resistance can be assessed by a Pourbaix diagram that indicates the regimes of corrosion product stability in terms of corrosion potential over a range of PH values as presented in Fig. 7.
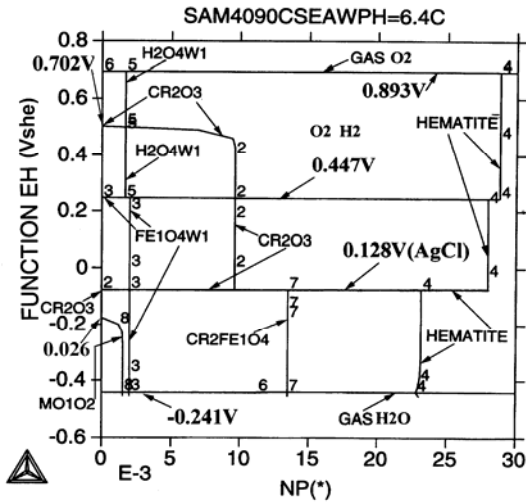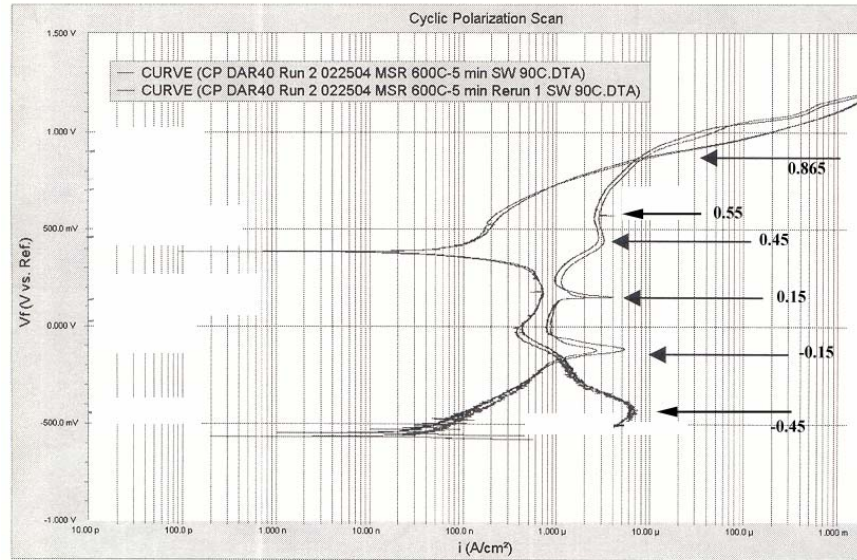

Figure 6. Calculated Voltage ,EH vs Phase Fraction relations at 90C in Seawater, at pH=6.4 for SAM 40.
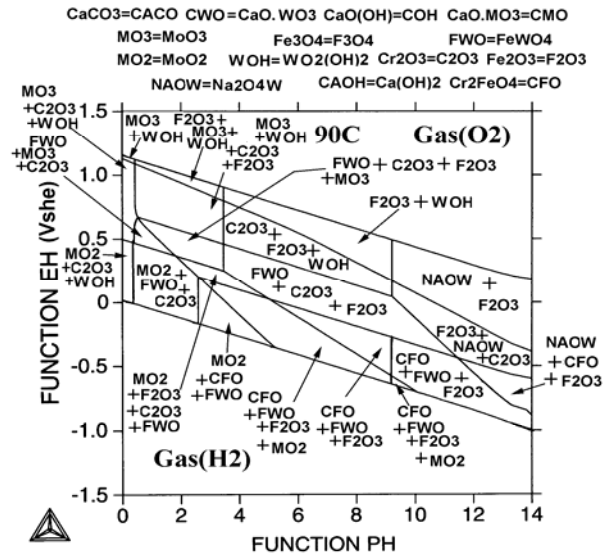
Figure 7. Calculated Pourbaix Diagram at 90C in Seawater for SAM 40.

The experimental validation of the computational analysis is presented in Fig. 8 that demonstrates the good agreement between the calculation model and the actual performance [3]. The specific features of the measured voltages can be compared with the calculated values. This sample was annealed at 600C for 5 minutes. The comparison yields the following: 0.865 Volts compares with the calculated formation of O_2 gas as the voltage is increased above 0.893Volts, 0.55Volts compares with the calculated dissolution of Cr_2O_3 as the voltage increases above 0.702 Volts. The observed anodic peak at 0.45Volts compares with the calculated transformation at 0.447 Volts of $FeO.WO_3$ to $WO_2.(OH)_2$ and Fe_2O_3 as voltage is increased. Similarly the anodic peak at 0.15 Volts compares well with the calculated transformation of Cr_2O_3 plus Fe_2O_3 to Cr_2FeO_4 at 0.128 Volts as the voltage decreases. The next prominent peak appears at -0.15 Volts which compares with the calculated dissolution of MoO_2 at 0.026 Volts as the voltage increases. Finally the anodic peak -0.45Volts compares with the calculated formation of H_2O gas at -0.241 Volts. Furthermore, the results in Fig. 8 demonstrate the superior corrosion resistance of amorphous Fe-based alloys.

Joint International Topical Meeting on Mathematics & Computation and
Supercomputing in Nuclear Applications (M&C + SNA 2007), Monterey, CA, 2007

8/13

Figure 8. Cyclic Polarization measurements for a melt spun ribbon (MSR) sample of Amorphous SAM 40.

Table I. Alloy compositions (at.%)

| Formulation	Fe	Cr	Mn	Mo	W	Y	B	C	Si
SAM35	54.5	15	2	2	1.5	---	16	4	5
SAM40	52.3	15	2	2.5	1.7	---	16	4	2.5
SAM2X5	49.7	18.1	1.9	7.4	1.6	---	15.2	3.8	2.4
SAM7	48	15	---	14	---	2	6	15	---

5. DESIGN OF RADIATION COMPATIBLE Fe-BASED GLASSES

The alloy composition SAM7 has been tailored to maximize glass forming ability and as such this alloy can form bulk metallic glass for cooling rates down to about 150 K/s without taking any special precautions to reduce impurity levels in the melt prior to processing. Since the glass-forming ability of most metallic glasses depend on having constituents with a range of atomic sizes to allow for optimal packing in the liquid state, modification of the alloy composition should be done in a manner as to preserve the original distribution of atoms of various size. As such, boron is added to SAM7 at the expense of carbon.

Thermocalc was applied to calculate the thermal characteristics of a series of modified SAM7 alloys and some compositions were selected for processing and thermal analysis (DTA). The thermal analysis results are shown in figure 8 and the results are summarized in table II, together with the calculated values. Generally, there is good agreement between the calculated values for the onset of melting, T_m and the liquidus temperature T_L when taking the multi-component nature of the alloy in consideration.

Based on this initial computational and experimental effort, one of the boron-modified alloys was selected for wedge casting to determine whether the critical cooling rate was effected by the substitution of carbon with boron. From traditional metrics concerning glass-forming

ability of alloys, such as reduced glass transition temperature T_{rg} (T_g/T_L) or range of supercooled liquid region T_x-T_L, it is expected that any of the modified alloys will exhibit a higher critical cooling rate for glass formation compared to the original alloy SAM7. Of the three alloys shown in figure 9, SAM7BX4 was chosen for wedge casting due to concern that the relatively high liquidus temperature of the other alloys would complicate the casting process.
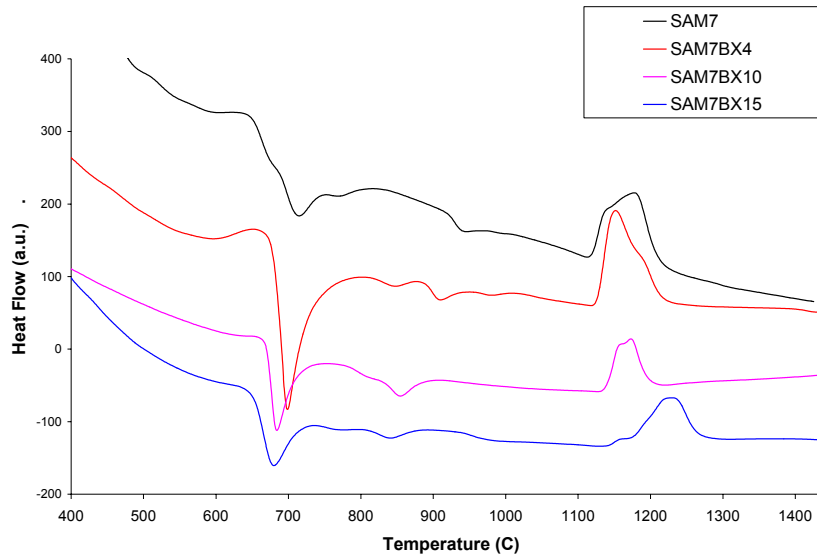

Figure 9. DTA heat flow traces acquired during continuous heating (40 K/min) for melt-spun ribbons for selected compositions. For details on the actual onset temperatures see table II.

Table II. Experimental and calculated thermal properties, with temperatures given in °C.

Formulation	T_{lim}	T_g	T_x	T_m (exp)	T_m (calc)	T_L (exp)	T_L (calc)
SAM7	586	585	640	1117	1097	1290	1340
SAMBX4	631	597	665	1125	1104	1341	1329
SAM7BX10	679	586	667	1137	1167	1374	1332
SAM7BX15	702	570	648	1147	1189	1420	1409

Wedge casting of alloys SAM7 and SAM7BX4 allows for a quantitative comparison between the cooling rates required to form a glassy phase upon quenching. Figures 9 and 10 show the transition zone in two wedge cast samples. The cooling rates are determined based on a combination of experimentally acquired cooling rates and a finite element heat transfer analysis. It is apparent from the micrographs depicted in figures 10 and 11 that the kinetic competition in the undercooled liquid is severely altered by the composition change. In alloy SAM7, it appears as if only one crystalline phase (previous studies strongly implies $M_{23}C_6$ structure) nucleates and eventually prevents vitrification. However, when 4 at% boron is added to the alloy at the expense of carbon, the kinetic competition is not dominated by a single phase rather than multiple phases. At the present time, the crystalline phases appearing in figure 11 have not been identified. The

critical cooling rate range for glass forming increases from about 160-230 K/s to 420-500 K/s. However, the latter range is well within the capability of a typical thermal spray process. As such, a modification of alloy composition to tailor the radiation compatibility has been successfully implemented by applying thermodynamic computational analysis as a guide to discovering promising alloy compositions that are evaluated by thermal analysis and wedge casting.
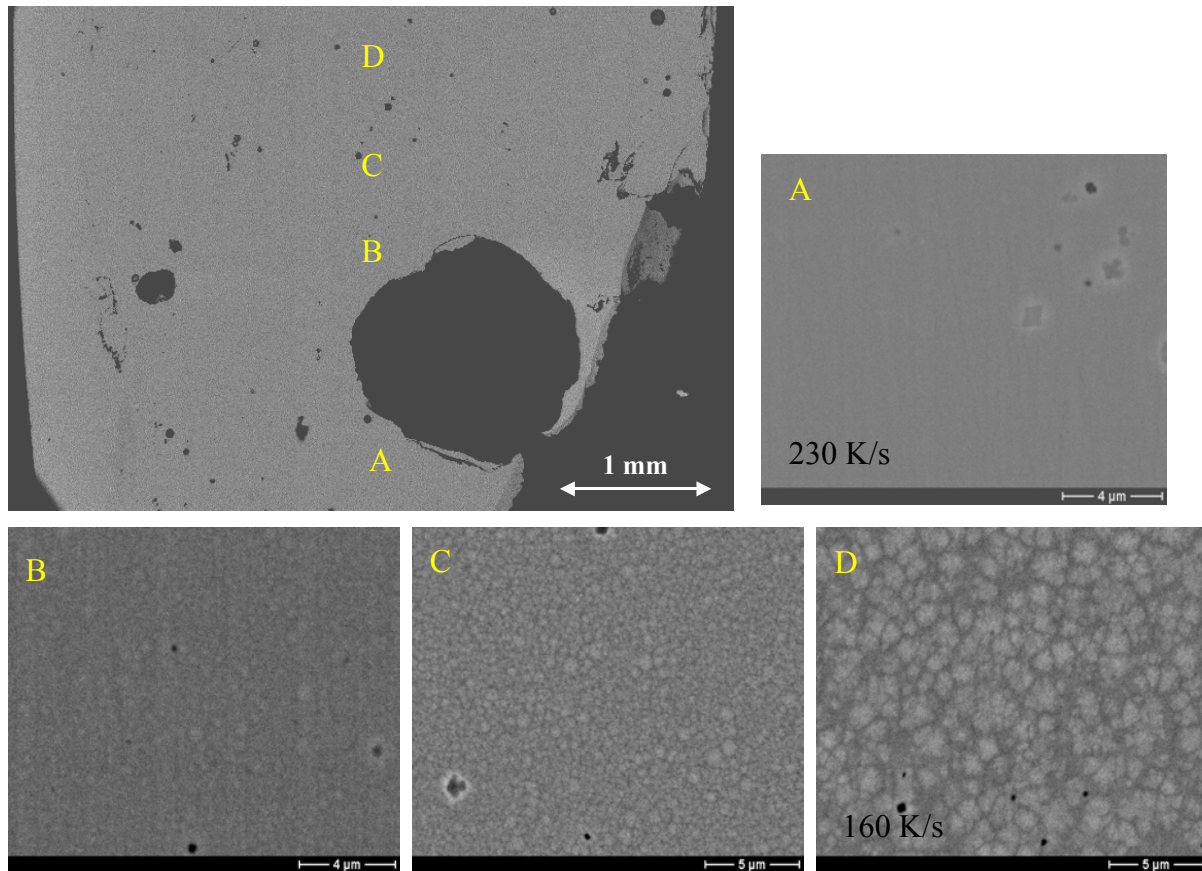

Figure 10 – Back-scattered electron (BSE) micrographs showing the transition region in SAM7 (upper left). Selected areas illustrates the gradual change of microstructure with decreasing cooling rate. Calculated cooling rates are indicated for region A (mostly amorphous) and D (mostly crystalline). The crystalline phase has a $M_{23}(B,C)_6$ structure [6]. The broken symmetry of the wedge is caused by the large spherical pore as well as a piece near the edge that fell of during sample preparation.

CONCLUSIONS

The design of advanced bulk Fe-based glass forming alloys requires the incorporation of multiple components in order to enable superior performance under multi-functional conditions and retain good glass forming. The computational thermodynamics and kinetics approaches that are being developed in the current work represent the state-of-the art for the analysis of complex

Joint International Topical Meeting on Mathematics & Computation and
Supercomputing in Nuclear Applications (M&C + SNA 2007), Monterey, CA, 2007

11/13

engineering alloys. At the same time the favorable experimental validation of the computational results indicates the merit in the underlying analysis.
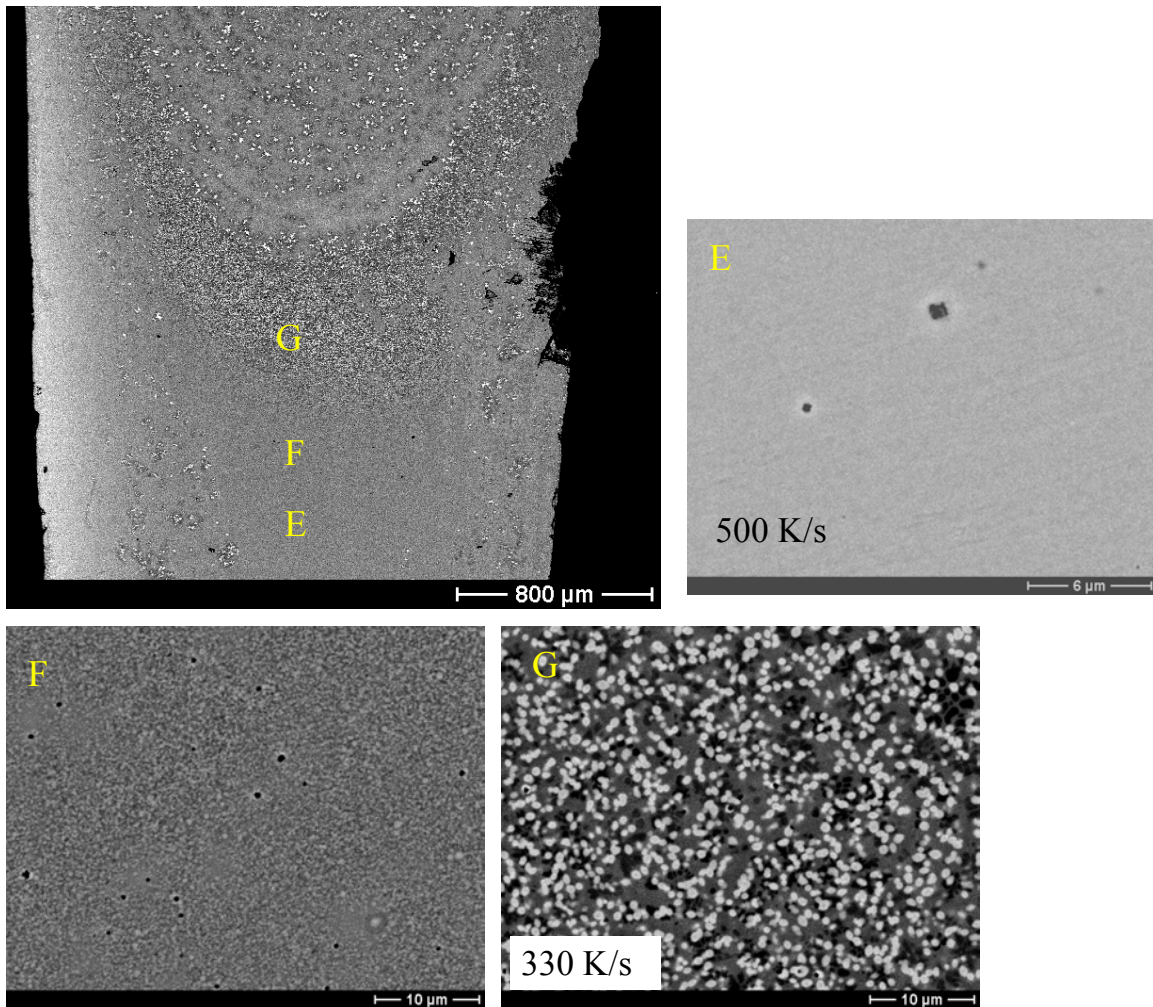
Figure 11 – BSE micrographs of the transition region in SAM7BX4. Calculated cooling rates are indicated for region E and G. Note how the transition zone reflects the C-shaped temperature contours that is characteristic of the mold geometry.

ACKNOWLEDGMENTS

Joint International Topical Meeting on Mathematics & Computation and
Supercomputing in Nuclear Applications (M&C + SNA 2007), Monterey, CA, 2007

12/13

REFERENCES

1. J.H. Perepezko and K. Hildal "Analysis of solidification microstructure during wedge-casting," *Philosophical Magazine*, **86**, pp.3681-3701 (2006).
2. K. Hildal, N. Sekido and J.H. Perepezko, "Critical cooling rate for $Fe_{48}Cr_{15}Mo_{14}Y_2C_{15}B_6$ bulk metallic glass formation", *Intermetallics*, **14**, pp.898-902 (2006).
3. H. J. Fecht, *J. Appl. Phys.*, **68**, 4494-4502, 1990.
4. W. J. Boettinger and J. H. Perepezko in *Rapidly solidified alloys: Processes, structures, properties, applications*. Eds. H. H. Liebermann, Decker, New York,17-78, 1993.
5. L. Battezzati and A. L. Greer, *Acta Met.*, **37**, (7), 1791-1802, 1989.
6. L. Battezzati, *Mat. Sci. Eng. A*, **375-377**, 60-65, 2004.
7. C. A. Angell, K. L. Ngai, G. B. McKenna, P. F. McMillan and S. W. Martin, *J. Appl. Phys.*, **88**, (6), 3113-3157, 2000.
8. A. Takeuchi and A. Inoue, *Mat. Sci. Eng. A.*, **375-377**, 449-454, 2004.
9. J. Farmer, J. Haslam et.al. "Corrosion characterization of iron-based high performance amorphous-metal thermal-spray coatings," *Proceedings of ASME PVP: Pressure vessels & piping division conference*, Denver, Colorado, July 17-21, (2005).

Joint International Topical Meeting on Mathematics & Computation and
Supercomputing in Nuclear Applications (M&C + SNA 2007), Monterey, CA, 2007

13/13